Editors' Suggestion

High-Temperature Ferroic Glassy States in $SrTiO_3$-Based Thin Films

Tianyu Li,[1,2,*] Shiqing Deng,[1,*,†] He Qi,[1,2] Tao Zhu,[3,4] Yu Chen,[5] Huanhua Wang,[5] Fangyuan Zhu,[6] Hui Liu,[1] Jiaou Wang,[5] Er-Jia Guo,[4] Oswaldo Diéguez,[7] and Jun Chen[1,2,8,‡]

[1]*Beijing Advanced Innovation Center for Materials Genome Engineering, University of Science and Technology Beijing, Beijing 100083, China*
[2]*Department of Physical Chemistry, University of Science and Technology Beijing, Beijing 100083, China*
[3]*Spallation Neutron Source Science Center, Dongguan 523803, China*
[4]*Beijing Synchrotron Radiation Facility, Institute of High Energy Physics, Chinese Academy of Sciences, Beijing 100049, China*
[5]*Beijing Synchrotron Radiation Facility, Institute of High Energy Physics, Chinese Academy of Sciences, Beijing 100049, China*
[6]*Shanghai Synchrotron Radiation Facility, Shanghai Advanced Research Institute, Chinese Academy of Sciences, Shanghai 201204, China*
[7]*Department of Materials Science and Engineering, Faculty of Engineering, Tel Aviv University, Tel Aviv 6997801, Israel*
[8]*Hainan University, Haikou 570228, China*

(Received 30 November 2022; revised 19 August 2023; accepted 24 October 2023; published 13 December 2023)

Disordered ferroics hold great promise for next-generation magnetoelectric devices because their lack of symmetry constraints implies negligible hysteresis with low energy costs. However, the transition temperature and the magnitude of polarization and magnetization are still too low to meet application requirements. Here, taking the prototype perovskite of $SrTiO_3$ as an instance, we realize a coexisting spin and dipole reentrant glass states in $SrTiO_3$ homoepitaxial films via manipulation of local symmetry. Room-temperature saturation magnetization and spontaneous polarization reach ~ 10 emu/cm^3 and ~ 25 μC/cm^2, respectively, with high transition temperatures (101 K and 236 K for spin and dipole glass temperatures and 556 K and 1100 K for Curie temperatures, respectively). Our atomic-scale investigation points out an underlying mechanism, where the Ti/O-defective unit cells break the local translational and orbital symmetry to drive the formation of unusual slush states. This study advances our understanding of the nature of the intricate couplings of ferroic glasses. Our approach could be applied to numerous perovskite oxides for the simultaneous control of the local magnetic and polar orderings and for the exploration of the underlying physics.

DOI: 10.1103/PhysRevLett.131.246801

Multiferroics, owing to the cross-coupling between various order parameters [ferroelectricity, (anti)ferromagnetic, ferroelasticity, and ferrotoroidicity], have gathered momentum as a new-type logic unit for information storage and processing [1–4]. Both type-I and type-II multiferroics (with different and same magnetoelectric origins) require a coexistence of long-range polar and magnetic orderings as a prerequisite to realize a linear magnetoelectric (ME) coupling [5,6]. However, the strict requirements regarding time and space inversion symmetry to engineer ME phenomena greatly limit their development given that it can only be possibly attainable in only 58 Shubnikov point groups from 69 magnetic groups [7]. This makes the eligible candidates extremely scarce, while their low ordering temperatures or coupling strengths can barely meet the application requirements. Furthermore, the first-order transition in long-range ordered ferroic crystals generally feature large hysteresis [8,9], raising concerns regarding energy loss and fatigue from the application perspective.

Ferroic glasses are representative of disordered or short-range ordering systems, which originate from local structural fluctuation and energetic competition. For example, spin glasses involve a local competition between exchange interactions that results in a metastable phase [10,11]. Similarly, owing to chaotic dipole interactions among the diverse polar nanoregions the dipole glass emerges in relaxor ferroelectrics [12,13]. In particular, due to the lack of long-range ordering, coexistence or cross-coupling of different types of ferroic glasses are free of the requirements for long-range symmetry breaking to achieve ME coupling [14,15]. This, therefore, brings the potential for diverse types of materials to be engineered as new ME candidates. On this basis, a high-order ME effect is enabled in materials where spin and dipole glasses coexist (type-III multiferroic) [16,17]. The prominent merits of type-III multiferroics such as small hysteresis and a wide temperature range for phase transition can provide promising applications in low-loss and power nonvolatile memory and sensor devices [18,19]. However, the disordered ferroics developed so far still face challenges, including generally low transition temperatures and weak magnetic and polar strength, still not comparable to long-range ferroics.

Herein, by modulating local symmetry in the canonical perovskite of $SrTiO_3$, we realize coexisting reentrant spin

and dipole glass (RSG and RDG) with high transition temperatures. The Curie temperatures for ferromagnetic (T_C^{FM}) and ferroelectric transition (T_C^{FE}) are as high as 556 and 1100 K, and the glass temperatures for spin (T_{RSG}) and dipole (T_{RDG}) are up to 101 and 236 K. It features strong RT saturation magnetization (M_s) of ~ 10 emu/cm^3 and spontaneous polarization (P_s) of ~ 25 μC/cm^2 compared to those in the $SrTiO_3$-based systems [20–22] and the disordered multiferroics [14,15,23,24]. Based on atomic-scale structure investigations, we correlate the glass states and frustration behaviors to the breaking in the local translational and orbital symmetry. It demonstrates that the purposely induced Ti/O-defect unit cells drive a local structure transition from the nonpolar cubic phase to the polar tetragonal-like phase, forming the nanosized polar slushes. The spin-glass state is thereby established due to the altered crystal-field splitting under the synergistic effect of Ti/O-defect unit cells and the resultant charge rearrangements. This methodology of introducing nanoscale M/O defects (M for transition metal) is generally applicable in wide-ranging perovskites for tailoring local polar and spin configurations, which would steer the exploration of new disordered multiferroics.

Nonstoichiometric $SrTiO_3$-based thin films with a Sr/Ti molar ratio of 1.22:1 were homoepitaxially grown on the (001)-oriented substrates via pulsed-laser deposition to induce the Ti/O defects (Supplemental Material, Figs. S1 and S2, Table S1) [25]. We first investigate the crystallographic structure and composition of the films. Figures 1(a) and 1(b) show the out-of-plane synchrotron x-ray diffraction (SXRD) pattern and (103)-spot reciprocal space map (RSM). The clear *Pendellösung* fringes suggest the high epitaxial quality of the film. The fitting in the inset in Fig. 1(a) suggests a homogeneous lattice constant c from the film-substrate interface to the top surface [26]. More importantly, (00L) peaks of the film are found to shift to lower L values compared to those of the substrate, indicating an enlarged c and increased c/a up to 1.039 for the film. This is corroborated by the atomic-scale aberration-corrected scanning transmission electron microscopy (STEM) characterizations. Figure 1(d) shows a high-angle annular dark-field (HAADF)-STEM image at [001] zone axis. Noteworthily, although the nonstoichiometry of Sr/Ti is purposely introduced the film maintains the perovskite structure, implying the presence of Ti vacancies. Whereas, quantitative analyses of the image can find the diffusely distributed nanoregions (<10 nm in size) with a marked lattice distortion and significantly increased c/a [Figs. 1(e) and S3] [107]. The composition of the film is investigated by Rutherford backscattering spectrometry (RBS) [108]. Figure 1(c) compares the RBS spectra of the film and stochiometric STO substrate, showing the identical RBS yields of the Ti element among them. While the Sr content in the film is higher than that

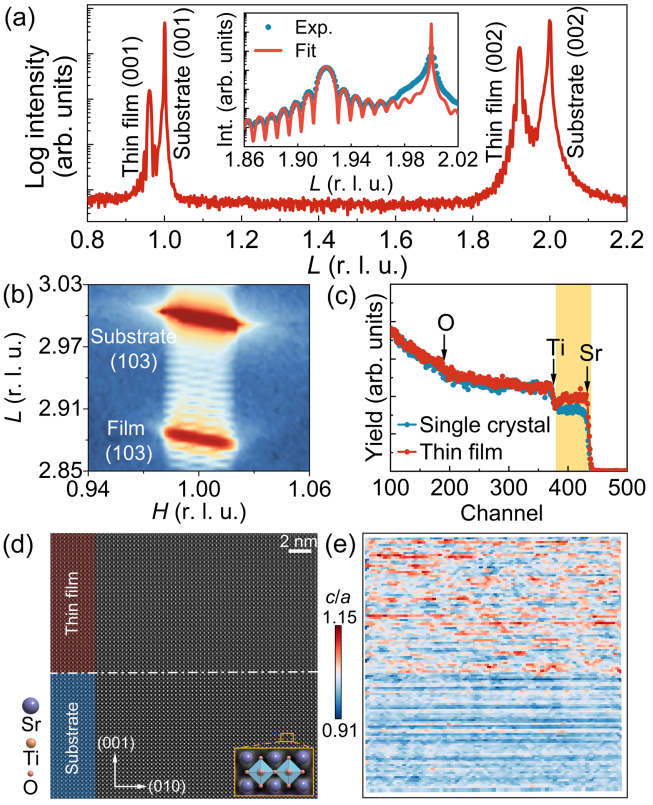

FIG. 1. (a) L-can SXRD pattern and the fitting result. (b) RSM around (103) spots. (c) RBS spectra for the film and bare $SrTiO_3$ crystal. (d) HAADF-STEM image, and (e) corresponding c/a map.

of the substrate, agreeing with the composition design and accounting for the formation of lattice-distorted nanoregions.

Theoretical studies have shown that the electronic configurations can be modulated by local lattice distortions to generate exotic magnetic states [109–111]. The magnetic properties of our structurally distorted films are shown in Fig. 2. RT magnetic field-dependent magnetization (M-H) loops correspond to a ferromagnetic state and an in-plane magnetic easy axis [Figs. 2(a) and S4]. The RT M_s is ~ 10 emu/cm^3 and also independent of film thicknesses (33, 47, 57, and 131 nm) (Fig. S5), which is higher than that of some magnet-substituted $SrTiO_3$ systems, such as $Sr(Ti_{0.95}, Mn_{0.05})O_3$ film (RT $M_s \sim 0.2$ emu/cm^3) [112]. This is confirmed by polarized neutron reflectometry (PNR) measurements. Figure 2(b) shows the RT reflectivity curves for parallel spin-up R^+ and antiparallel spin-down R^- with respect to wave vector transfer Q. The discrepancy between R^{++} and R^{--} reflectivity curves and resulting spin asymmetry oscillation in Q space indicates an intrinsic magnetic signal in the system (Supplemental Material, Fig. S6 [25]). Temperature-dependent magnetization (M-T) curves in Fig. 2(c) exhibit an obvious ferromagnetic-to-paramagnetic transition at T_C^{FM} of 556 K. More importantly, the zero-field cooling (ZFC) and field cooling (FC) curves

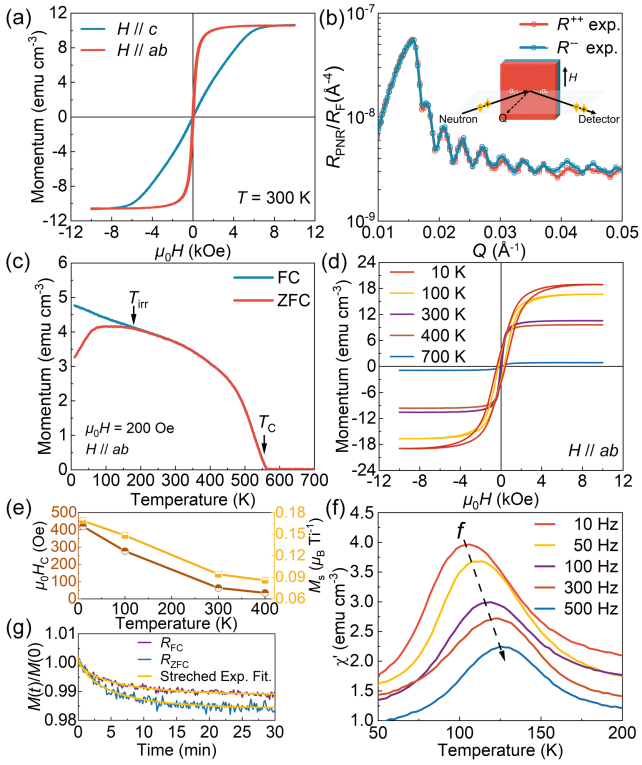

FIG. 2. (a) RT M-H curves of the film. (b) RT PNR spectra with an in-plane magnetic field of 1.0 T. The inset is an experimental schematic. (c) ZFC/FC M-T curves of the film. Temperature-dependent (d) M-H curves and (e) coercive field ($\mu_0 H_c$) and M_s. (f) ac susceptibility vs temperature curves under different frequencies. (g) Magnetic relaxation curves under R_{FC} and R_{ZFC} routes at 10 K and fitting lines.

manifest a clear bifurcation around the irreversible temperature (T_{irr}) of 170 K. Following the bifurcation shows a plateau of the ZFC curve at around 101 K. These features originate from the freezing of magnetic moments in the system [30]. This, along with the disorder-to-order, and order-to-glass transitions upon temperature decreasing, both indicate a RSG state at low temperatures [76,113]. In this regard, T_{RSG} is assigned to 101 K [115]. Typically, the RSG behavior can be attributed to the dominant ferromagnetic interaction prevailing over the antiferromagnetic component in frustrated systems [114]. In the transverse (xy) freezing model, spin clusters tend to align predominantly along a specific direction, while in the random-field model, they intertwine to form spin networks [45,115]. The small coercive field in the M-H loops would arise from the weak domain interactions [Figs. 2(d) and 2(e)]. Therefore, the ferromagneticlike state presented in RSG systems represents a macroscopic manifestation of the net spin components along a particular direction and, therefore, differs fundamentally from that of regular ferromagnets.

To further distinguish the spin-glass state and determine its dynamics, alternating current (ac) magnetic susceptibility and magnetic relaxation measurements were conducted. The former was performed in the temperature range of 50–200 K under different frequencies. Notably, the real (χ') and imaginary (χ'') components of the susceptibility show the frequency-dependent maximum values [Figs. 2(f) and S7], which is correlated to the frozen moment upon cooling [116,117]. With the increase in frequency, the peaks shift toward higher temperatures, arising from the prolonged action time due to the frozen delay and being consistent with the characteristics of a typical spin-glass state [116,117]. Two different time-dependent magnetic relaxation routes (R_{FC} and R_{ZFC}) were utilized to clarify the relaxation behavior of spin glass [Fig. 2(g)] [28]. Both show a decreased magnetization upon unloading the field, that is, the aging effect, which is another characteristic of the spin glass other than the superparamagnetic state. The relaxation curves can be fitted by a modified stretched function model (Table S2), suggesting that the system consists of a spin-glass state with an accompanied ferromagnetism background [29–31].

The macroscopic polarization of the film was characterized by polarization-electric field (P-E) loop and frequency-dependent dielectric spectra measurements. Figure 3(a) shows the RT P-E loop, wherein a slim shape implies a dipole glass state [118]. Notably, the P_s determined from the loop reaches up to $\sim 25\ \mu C/cm^2$, which agrees with our previous report and rivals conventional ferroelectrics like $BaTiO_3$ ($P_s \sim 26\ \mu C/cm^2$) [35,119]. Besides, a large resistivity of $\sim 10^{10}\ \Omega$ cm and low dielectric loss (~ 0.01–0.02 at 10^2–10^5 Hz) rule out any significant conductive contribution [insets in Figs. 3(a) and Supplemental Material, Fig. S8 [25]]. Temperature-dependent XRD and dielectric spectra further confirm this frustration state [Figs. 3(b) and 3(c)]. As the temperature increases, a ferroelectric transition occurs at $T_C^{FE} \sim 1100$ K, as evidenced by a sudden shift of the (002) peak of the film to a higher angle at this temperature [Fig. 3(b)], which surpasses that of many prototypical ferroelectrics like $BaTiO_3$ ($T_C^{FE} \sim 403$ K) and $PbTiO_3$ ($T_C^{FE} \sim 763$ K) [119,120]. Notably, we observed a distinct dielectric anomaly in conjunction with a noticeable frequency dependence in dielectric spectra [Fig. 3(c)]. This, along with the ferroelectric-to-paraelectric transition at T_C^{FE}, indicates a RDG state similar to the reentrant behavior of spin glass [115]. By employing the Vogel-Fulcher law [32], the T_{RDG} can be determined to 236 K (Table S3). Below this critical temperature, the dipole-dipole interactions become significantly enhanced due to the reduced thermal activation. Consequently, the polar nanoclusters freeze into a nonergodic state, exhibiting behavior analogous to spin glass [114]. We compare these transition temperatures for multiglass states with representative disordered multiferroics [Fig. 3(d) and Supplemental Material, Figs. S9 and S10] [14,15,23,24]. Considerable effort has been devoted to studying $SrTiO_3$, a model perovskite system, to introduce magnetic or electric dipole moments [20–22].

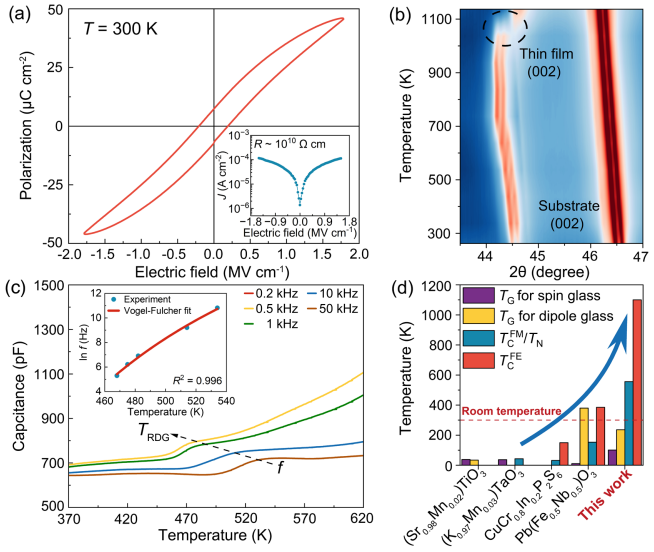

FIG. 3. (a) P-E loop and leakage current curve. (b) Temperature-dependent XRD patterns of (002) peaks. (c) Temperature–frequency-dependent dielectric spectra and Vogel-Fulcher fitting results. (d) Comparison of transition temperatures in this work with those of the representative disordered ferroics [14,15,23,24].

However, the achieved properties remain inferior regarding the relatively low magnitude of transition temperature or moments. Remarkably, the thin films investigated in this study exhibit dipole and spin ordering temperatures that are significantly higher than RT and surpass those observed in representative disordered multiferroics and $SrTiO_3$-based systems.

To probe the structural origin of these glass states, annular bright-field (ABF) imaging was performed, where both heavy and light atoms are visible. As shown in Fig. 4(a), randomly distributed nanoregions with blurred contrast are observed, which is consistent with the observations in the HAADF-STEM image and should arise from the strain-induced dechanneling effect [121]. Quantitative analysis of the atomic column intensities reveals a notable decrease in the intensity of the Ti/O atom columns within contrast-blurred nanoregions compared to the normal region or substrate [Figs. 4(b) and S11]. This observation suggests that the excess Sr atoms in the film do not form SrO cluster or Ruddlesden-Popper structure but instead induce Ti/O vacancies, which should have their origin in the control of chemical composition and deposition thermodynamics [122]. By mapping the polarization of the unit cell and correlating it with the variations in atomic intensity, it becomes evident that these Ti/O-defect unit cells are responsible for the local symmetry breaking. Specifically, the Ti/O-defect nanoregions exhibit a significant lattice distortion and polar displacement [Figs. 4(c) and 4(d)]. The polarizations of these high-density nanoregions manifest relatively random directions and slushlike configurations with sizes of 2–10 nm, both of which contribute to the observed frustration states.

The evolution of electronic structure was further revealed by x-ray photoelectron spectroscopy (XPS), electron energy-loss spectroscopy (EELS), x-ray linear dichroism (XLD), and x-ray magnetic circular dichroism (XMCD). No additional XPS peaks from the contamination or impurity of magnetic elements other than characteristic lines for Sr, Ti, and O elements can be detected in the overall spectra (Supplemental Material, Fig. S12 [25]). A clear shift of the Ti $2p$ peak indicates the existence of Ti^{3+} ions in the film, being consistent with the STEM results. In Figs. 4(e) and 4(f), Ti L-edge and O K-edge EELS spectra are analyzed to clarify the changes in local electronic structure. Noteworthily, peaks that correspond to the t_{2g} and e_g orbitals for the films are broadened and the crystal-field splitting energy is decreased. This corresponds to the local symmetry breaking and resultant polar displacements that further break the energy-level degeneracy of the $3d$ orbital groups. That is, driven by the off-centering movement of Ti atoms in the c-axis elongated TiO_6 octahedral, the hybridization between $3d_{3z^2-r^2}$ and O $2p$ orbitals is reinforced [Figs. 4(g) and S13]. This double confirms the polar displacements observed in Fig. 4(d). For example, doubly degenerated orbitals of $3d_{x^2-y^2}$ and $3d_{3z^2-r^2}$ will split, when the hybridization between $3d_{3z^2-r^2}$ and $2p$ orbitals is enhanced by the off-center Ti atom. This agrees with the previous study and indicates the polar displacement of Ti atoms in the tetragonal-distorted TiO_6 octahedra [123]. Furthermore, Ti $L_{3,2}$-edge XLD signals show a distinct $3d$-orbital asymmetry between the in-plane ($3d_{x^2-y^2}$ and $3d_{xy}$) and out-of-plane components ($3d_{3z^2-r^2}$, $3d_{xz}$, and $3d_{yz}$) [Fig. 4(h)]. This suggests the anisotropy of hybridization strength due to the lattice distortions [124], which can be the driving force for the emergence of local spontaneous polarization.

In the film with a dipole glass state, exotic polar spin orderings can be possibly provoked by either local lattice strain or Ti/O defects [123,125–127]. Notably, ab-plane e_g $3d_{x^2-y^2}$ orbital has fewer empty states compared to out-of-plane $3d_{3z^2-r^2}$ orbital [Fig. 4(h)], indicating the unpaired electrons preferentially occupied in the in-plane orbitals with $3d^1$ configuration. This suggests that the Ti/O defect-induced off-center displacement of Ti leads to a tetragonal distortion of the bulk cubic unit cell of $SrTiO_3$ (Fig. S13 [25]). These local dipoles then interact to form a dipolar glass. Meanwhile, the same Ti/O defect-based mechanism is responsible for a deviation in Ti valence from the bulk 4+ ($3d^0$) to 3+ ($3d^1$) valency, consequently generating local magnetic dipoles that couple to a magnetic glass. Importantly, the magnetic moment of Ti is confirmed by Ti $L_{3,2}$-edge XMCD, wherein the asymmetric RT XMCD signal between L_3 and L_2 edge evidences its presence [Fig. 4(i)]. This confirms that the Ti/O-defective unit cells within the nanoregion can serve as seeds to induce spin-glass behaviors, being alike to the role of randomly

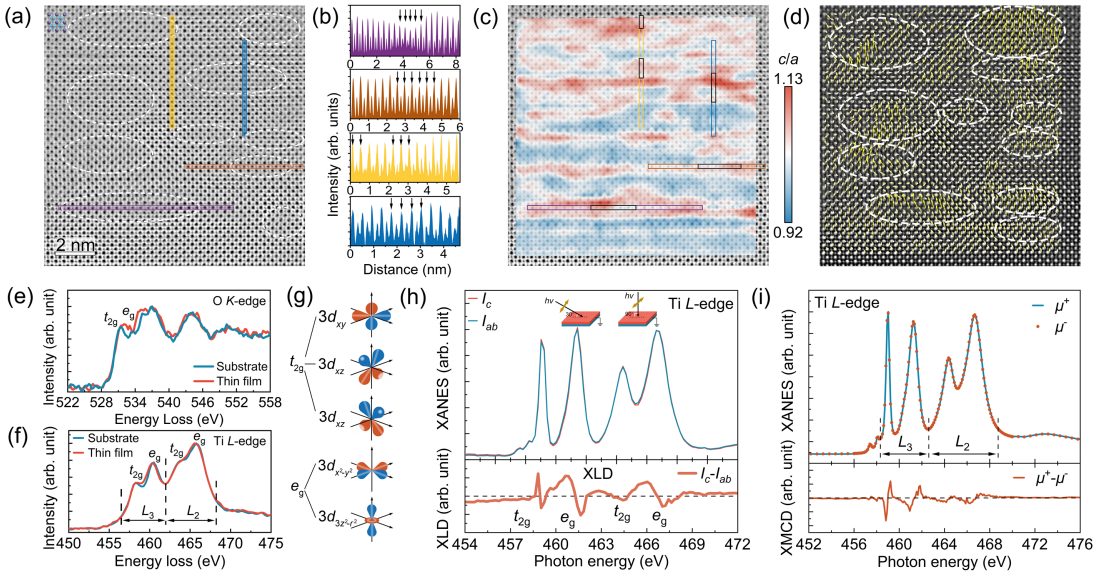

FIG. 4. (a) ABF-STEM image of the film at [100] zone axis. (b) Intensity profiles of Ti/O and O atom columns. Colored profiles correspond to the regions selected in (a) with the same color. Black arrows denote the Ti/O-deficient atomic columns. (c) *c*/*a* and (d) polar displacement maps overlaid on the contrast-inverted image. Black boxes denote the corresponding Ti/O-defect columns marked by arrows in (b). (e) O *K*-edge and (f) Ti $L_{3,2}$-edge EELS spectra for the film and substrate. (g) Schematics of Ti 3*d* orbitals. (h) Ti $L_{3,2}$-edge XLD spectra. The inset shows the experimental configuration, where the x-ray polarization orientation is denoted by the yellow arrows. (i) RT Ti $L_{3,2}$-edge XMCD spectra, where μ^+/μ^- denotes left-hand and right-hand circular x-ray polarization.

substituted magnetic elements in diluted magnetic compounds. The difference lies in that the magnitude of local structure and symmetry modulated by the exotic substitution to the host system is relatively limited [16]. Both lattice distortion and magnetic or electric properties exhibit independence from film thickness, evidencing the unique role of Ti/O defects in the modulation of local symmetry. Given that the dipole and spin glass states as well as the lattice variation share the same origin, the charge, spin, and lattice degrees of freedom are essentially closely correlated at the atomic scale. This, therefore, would enable the interactions between them for high-temperature multiple glass states with the coexistence and cross-coupling of different orderings. The anomalies in the permittivity near the T_{irr} suggest a potential magnetoelectric correlation in the film (Fig. S14 [25]).

In conclusion, coexisting high-temperature reentrant spin and dipole glass states have been realized in the nonstoichiometric $SrTiO_3$ films via manipulation of local lattice symmetry. With the introduction of Ti/O nanodefects, the local symmetry lowers from a high-symmetry cubic phase to a tetragonal-like structure with markedly changed electronic configurations. Accordingly, slushlike dipole and spin glass states are engendered and show close correlations. Similar *M*/O (*M* for metal) defects could also be designed in widespread perovskites for the modulation of local structure, orbital asymmetry, and electronic redistribution for the glass behaviors. This study delivers a new methodology to break local energy balance and to arouse dipole and spin fluctuations, providing fundamental ingredients for the design of emergent physical attributes such as disordered multiferroics with the high-order magnetoelectric effect.

This work was supported by the National Natural Science Foundation of China (Grants No. 21825102, No. 22235002, and No. 22161142022) and the China National Postdoctoral Program for Innovative Talents (Grant No. BX20200043). The research at Tel Aviv University is financially supported by the Israel Science Foundation (Grant No. 3433/21). This study used the resources of the Beijing National Center for Electron Microscopy at Tsinghua University, China Spallation Neutron Source of the Chinese Academy of Sciences (CAS), Beijing Synchrotron Radiation Facility (1W1A and 4B9B beamlines) of CAS, and Shanghai Synchrotron Radiation Facility (BL07U and BL02U2 beamlines) of CAS. The authors appreciate Dr. Céline Lichtensteiger at the University of Geneva for the help in XRD fitting.

The authors declare no competing interests.

*T. L. and S. D. contributed equally to this work.
†Corresponding author: sqdeng@ustb.edu.cn
‡Corresponding author: junchen@ustb.edu.cn

[1] J. A. Mundy *et al.*, Nature (London) **537**, 523 (2016).
[2] S. Das *et al.*, Nature (London) **568**, 368 (2019).

[3] S. Manipatruni, D. E. Nikonov, C.-C. Lin, T. A. Gosavi, H. Liu, Bhagwati Prasad, Y.-L. Huang, E. Bonturim, R. Ramesh, and I. A. Young, Nature (London) **565**, 35 (2019).
[4] N. A. Spaldin and R. Ramesh, Nat. Mater. **18**, 203 (2019).
[5] D. Khomskii, Physics **2**, 20 (2009).
[6] S. Dong, J.-M. Liu, S.-W. Cheong, and Z. Ren, Adv. Phys. **64**, 519 (2015).
[7] M. Fiebig, J. Phys. D **38**, R123 (2005).
[8] V. Wadhawan, *Introduction to Ferroic Materials* (CRC Press, Boca Raton, FL, 2000).
[9] S. Yang, X. Ren, and X. Song, Phys. Rev. B **78**, 174427 (2008).
[10] M. Mézard, G. Parisi, N. Sourlas, G. Toulouse, and M. Virasoro, Phys. Rev. Lett. **52**, 1156 (1984).
[11] M. Baity-Jesi *et al.*, Phys. Rev. Lett. **118**, 157202 (2017).
[12] L. E. Cross, Ferroelectrics **76**, 241 (1987).
[13] D. Viehland, M. Wuttig, and L. E. Cross, Ferroelectrics **120**, 71 (1991).
[14] V. V. Shvartsman, S. Bedanta, P. Borisov, W. Kleemann, A. Tkach, and P. M. Vilarinho, Phys. Rev. Lett. **101**, 165704 (2008).
[15] W. Kleemann, V. V. Shvartsman, P. Borisov, and A. Kania, Phys. Rev. Lett. **105**, 257202 (2010).
[16] W. Kleemann, Solid State Phenom. **189**, 41 (2012).
[17] H. Zabel and M. Farle, *Magnetic Nanostructures: Spin Dynamics and Spin Transport* (Springer, New York, 2012), Vol. 246.
[18] T. Lookman and X. Ren, *Frustrated Materials and Ferroic Glasses* (Springer, New York, 2018), Vol. 275.
[19] H. Xu, S. Xu, X. Xu, J. Zhuang, W. Hao, and Y. Du, Microstructure **2**, 2022011 (2022).
[20] A. S. Kumar, P. Suresh, M. M. Kumar, H. Srikanth, M. L. Post, K. Sahner, R. Moos, and S. Srinath, J. Phys. Conf. Ser. **200**, 092010 (2010).
[21] M. Valent, T. Kolodiazhnyi, I. Arčon, F. Aguesse, A. K. Axelsson, and N. M. Alford, Adv. Funct. Mater. **22**, 2114 (2012).
[22] A. D. Rata *et al.*, APL Mater. **10**, 091108 (2022).
[23] V. V. Shvartsman, S. Bedanta, P. Borisov, W. Kleemann, A. Tkach, and P. M. Vilarinho, J. Appl. Phys. **107**, 103926 (2010).
[24] W. Kleemann, V. V. Shvartsman, P. Borisov, J. Banys, and Y. M. Vysochanskii, Phys. Rev. B **84**, 094411 (2011).
[25] See Supplemental Material at http://link.aps.org/supplemental/10.1103/PhysRevLett.131.246801, which includes Refs. [26–106], for detailed descriptions of (1) sample synthesis; (2) structure characterizations and chemical composition analysis; (4) exclusion of magnetic impurities and other artifacts; (5) magnetic and electric measurements; (6) optimization of chemical composition.
[26] C. Lichtensteiger, J. Appl. Crystallogr. **51**, 1745 (2018).
[27] S. J. Pennycook and D. E. Jesson, Ultramicroscopy **37**, 14 (1991).
[28] B. Pang, L. Zhang, Y. B. Chen, J. Zhou, S. Yao, S. Zhang, and Y. Chen, ACS Appl. Mater. Interfaces **9**, 3201 (2017).
[29] R. V. Chamberlin, G. Mozurkewich, and R. Orbach, Phys. Rev. Lett. **52**, 867 (1984).
[30] J. A. Mydosh, *Spin Glasses: An Experimental Introduction* (CRC Press, London, 1993).
[31] M. Gabay and G. Toulouse, Phys. Rev. Lett. **47**, 201 (1981).
[32] A. K. Tagantsev, Phys. Rev. Lett. **72**, 1100 (1994).
[33] C. Long, W. Zhou, H. Song, K. Zheng, W. Ren, H. Wu, X. Ding, and L. Liu, Acta Mater. **256**, 119135 (2023).
[34] B. R. Coles, B. V. B. Sarkissian, and R. H. Taylor, Philos. Mag. B **37**, 489 (1978).
[35] T. Li, S. Deng, H. Liu, S. Sun, H. Li, S. Hu, S. Liu, X. Xing, and J. Chen, Adv. Mater. **33**, 2008316 (2021).
[36] D. Damjanovic, Rep. Prog. Phys. **61**, 1267 (1998).
[37] J. Kroder *et al.*, Phys. Rev. B **99**, 174410 (2019).
[38] Y. Nakai, M. Sakuma, and N. Kunitomi, J. Phys. Soc. Jpn. **56**, 301 (1987).
[39] S. Sharma, E. P. Amaladass, and A. Mani, Mater. Des. **131**, 204 (2017).
[40] A. Haldar, K. G. Suresh, and A. K. Nigam, Europhys. Lett. **91**, 67006 (2010).
[41] C. Tien, J. J. Lu, and L. Y. Jang, Phys. Rev. B **65**, 214416 (2002).
[42] P. Bag, P. R. Baral, and R. Nath, Phys. Rev. B **98**, 144436 (2018).
[43] P. Gibbs, T. M. Harders, and J. H. Smith, J. Phys. F **15**, 213 (1985).
[44] P. R. T. Ribeiro, F. L. A. Machado, D. C. Harrison, E. D. Dahlberg, and S. M. Rezende, J. Magn. Magn. Mater. **541**, 168537 (2022).
[45] G. Aeppli, S. M. Shapiro, R. J. Birgeneau, and H. S. Chen, Phys. Rev. B **28**, 5160 (1983).
[46] K. Jonason, J. Mattsson, and P. Nordblad, Phys. Rev. B **53**, 6507 (1996).
[47] H. Yamahara, M. Seki, M. Adachi, M. Takahashi, H. Nasu, K. Horiba, H. Kumigashira, and H. Tabata, J. Appl. Phys. **118**, 063905 (2015).
[48] H. Shiraishi, M. Sugamura, and T. Hori, J. Magn. Magn. Mater. **70**, 230 (1987).
[49] T. Samanta, P. A. Bhobe, A. Das, A. Kumar, and A. K. Nigam, Phys. Rev. B **97**, 184421 (2018).
[50] L. Xue, L. Shao, Q. Luo, and B. Shen, J. Alloys Compd. **790**, 633 (2019).
[51] H. Zeng, G. Yu, Y. Yuan, W. Wang, X. Luo, C. Chen, S. U. Rehman, G. Yuan, S. Ma, and Z. Zhong, J. Magn. Magn. Mater. **521**, 167532 (2021).
[52] Q. Zhang, D. Li, W. B. Cui, J. Li, and Z. D. Zhang, J. Appl. Phys. **106**, 113915 (2009).
[53] T. Gao, K. Nishimura, T. Namiki, and H. Okimoto, J. Appl. Phys. **111**, 013913 (2012).
[54] D. X. Li, S. Nimori, Y. Shiokawa, A. Tobo, H. Onodera, Y. Haga, E. Yamamoto, and Y. Ōnuki, Appl. Phys. Lett. **79**, 4183 (2001).
[55] B. Maji, K. G. Suresh, and A. K. Nigam, J. Phys. Condens. Matter **23**, 506002 (2011).
[56] P. Liao *et al.*, Appl. Phys. Lett. **104**, 092410 (2014).
[57] A. K. Nayak, K. G. Suresh, and A. K. Nigam, J. Phys. Condens. Matter **23**, 416004 (2011).
[58] S. Chatterjee, S. Giri, S. K. De, and S. Majumdar, Phys. Rev. B **79**, 092410 (2009).
[59] M. K. Ray, K. Bagani, P. K. Mukhopadhyay, and S. Banerjee, Europhys. Lett. **109**, 47006 (2015).
[60] Y. J. Zhang, Q. Q. Zeng, Z. Y. Wei, Z. P. Hou, Z. H. Liu, E. K. Liu, X. K. Xi, W. H. Wang, X. Q. Ma, and G. H. Wu, J. Alloys Compd. **749**, 134 (2018).

[61] W. Abdul-Razzaq and J. S. Kouvel, J. Appl. Phys. **55**, 1623 (1984).
[62] S. C. Ho, I. Maartense, and G. Williams, J. Appl. Phys. **53**, 2235 (1982).
[63] E. A. Goremychkin, R. Osborn, B. D. Rainford, R. T. Macaluso, D. T. Adroja, and M. Koza, Nat. Phys. **4**, 766 (2008).
[64] V. K. Anand, D. T. Adroja, and A. D. Hillier, Phys. Rev. B **85**, 014418 (2012).
[65] S. Pakhira, C. Mazumdar, R. Ranganathan, and S. Giri, J. Alloys Compd. **742**, 391 (2018).
[66] B. S. Wang, P. Tong, Y. P. Sun, X. B. Zhu, Z. R. Yang, W. H. Song, and J. M. Dai, Appl. Phys. Lett. **97**, 042508 (2010).
[67] J. J. Hauser, Phys. Rev. B **34**, 3212 (1986).
[68] D. X. Li, T. Yamamura, S. Nimori, K. Yubuta, and Y. Shiokawa, Appl. Phys. Lett. **87**, 142505 (2005).
[69] D. Kaczorowski and H. Noël, J. Phys. Condens. Matter **5**, 9185 (1993).
[70] D. X. Li, S. Nimori, T. Yamamura, and Y. Shiokawa, J. Appl. Phys. **103**, 07B715 (2008).
[71] D. X. Li, Y. Shiokawa, Y. Homma, A. Uesawa, A. Dönni, T. Suzuki, Y. Haga, E. Yamamoto, T. Honma, and Y. Ōnuki, Phys. Rev. B **57**, 7434 (1998).
[72] S. Thota and M. S. Seehra, J. Appl. Phys. **113**, 203905 (2013).
[73] M. D. Mukadam, S. M. Yusuf, P. Sharma, S. K. Kulshreshtha, and G. K. Dey, Phys. Rev. B **72**, 174408 (2005).
[74] P. Schiffer, A. P. Ramirez, D. A. Huse, P. L. Gammel, U. Yaron, D. J. Bishop, and A. J. Valentino, Phys. Rev. Lett. **74**, 2379 (1995).
[75] S. H. Song, M. H. Jung, and S. H. Lim, J. Phys. Condens. Matter **19**, 036211 (2007).
[76] J. Dho, W. S. Kim, and N. H. Hur, Phys. Rev. Lett. **89**, 027202 (2002).
[77] P. A. Kumar, R. Mathieu, P. Nordblad, S. Ray, O. Karis, G. Andersson, and D. D. Sarma, Phys. Rev. X **4**, 011037 (2014).
[78] A. Malinowski, V. L. Bezusyy, R. Minikayev, P. Dziawa, Y. Syryanyy, and M. Sawicki, Phys. Rev. B **84**, 024409 (2011).
[79] J. Wu and C. Leighton, Phys. Rev. B **67**, 174408 (2003).
[80] J. K. Murthy and A. Venimadhav, J. Appl. Phys. **113**, 163906 (2013).
[81] J. Pérez, J. García, J. Blasco, and J. Stankiewicz, Phys. Rev. Lett. **80**, 2401 (1998).
[82] M. Viswanathan and P. S. A. Kumar, Phys. Rev. B **80**, 012410 (2009).
[83] M. Tachibana, T. Tojo, H. Kawaji, T. Atake, H. Ikuta, Y. Uchimoto, and M. Wakihara, Phys. Rev. B **66**, 092406 (2002).
[84] X. Bie, Y. Gao, X. Yang, Y. Wei, H. Ehrenberg, M. Hinterstein, G. Chen, C. Wang, and F. Du, J. Alloys Compd. **626**, 150 (2015).
[85] H. Yamahara, M. Seki, and H. Tabata, J. Magn. Magn. Mater. **501**, 166437 (2020).
[86] Y. Muraoka, H. Tabata, and T. Kawai, Appl. Phys. Lett. **76**, 1179 (2000).
[87] Y. Muraoka, H. Tabata, and T. Kawai, Appl. Phys. Lett. **77**, 4016 (2000).
[88] P. Bag, K. Somesh, and R. Nath, J. Magn. Magn. Mater. **497**, 165977 (2020).
[89] W. J. Feng, D. Li, W. J. Ren, Y. B. Li, W. F. Li, J. Li, Y. Q. Zhang, and Z. D. Zhang, Phys. Rev. B **73**, 205105 (2006).
[90] J. Kroder, J. Gooth, W. Schnelle, G. H. Fecher, and C. Felser, AIP Adv. **9**, 055327 (2019).
[91] J. Blasco and J. García, Phys. Rev. B **51**, 3569 (1995).
[92] A. K. Singh, S. Chauhan, and R. Chandra, Appl. Phys. Lett. **110**, 102402 (2017).
[93] M. Svedberg, S. Majumdar, H. Huhtinen, P. Paturi, and S. Granroth, J. Phys. Condens. Matter **23**, 386005 (2011).
[94] A. Poddar and C. Mazumdar, J. Appl. Phys. **106**, 093908 (2009).
[95] B. Yuan, J. Yang, X. Z. Zuo, D. P. Song, X. W. Tang, X. B. Zhu, J. M. Dai, W. H. Song, and Y. P. Sun, J. Appl. Phys. **117**, 233906 (2015).
[96] Q.-Q. Gao, J.-B. Li, G.-N. Li, G.-H. Rao, J. Luo, G.-Y. Liu, and J.-K. Liang, J. Appl. Phys. **114**, 053901 (2013).
[97] T. Chakrabarty, A. V. Mahajan, and S. Kundu, J. Phys. Condens. Matter **26**, 405601 (2014).
[98] X. H. Zhang, Q. Yuan, J. C. Han, J. G. Zhao, J. K. Jian, Z. H. Zhang, and B. Song, Appl. Phys. Lett. **103**, 022405 (2013).
[99] B. Song, J. Jian, H. Bao, M. Lei, H. Li, G. Wang, Y. Xu, and X. Chen, Appl. Phys. Lett. **92**, 192511 (2008).
[100] T. Scholz and R. Dronskowski, AIP Adv. **6**, 055107 (2016).
[101] N. B. Brandt and V. V. Moshchalkov, Adv. Phys. **33**, 193 (1984).
[102] A. Mauger, J. Ferré, M. Ayadi, and P. Nordblad, Phys. Rev. B **37**, 9022 (1988).
[103] Y. Iijima, Y. Kamei, N. Kobayashi, J. Awaka, T. Iwasa, S. Ebisu, S. Chikazawa, and S. Nagata, Philos. Mag. **83**, 2521 (2003).
[104] H. Maletta, J. Appl. Phys. **53**, 2185 (1982).
[105] J. M. Rojo, J. L. Mesa, L. Lezama, J. L. Pizarro, M. I. Arriortua, J. R. Fernandez, G. E. Barberis, and T. Rojo, Phys. Rev. B **66**, 094406 (2002).
[106] S. Zapf, H. S. Jeevan, T. Ivek, F. Pfister, F. Klingert, S. Jiang, D. Wu, P. Gegenwart, R. K. Kremer, and M. Dressel, Phys. Rev. Lett. **110**, 237002 (2013).
[107] C. T. Nelson *et al.*, Nano Lett. **11**, 828 (2011).
[108] C. Jeynes, N. P. Barradas, and E. Szilágyi, Anal. Chem. **84**, 6061 (2012).
[109] H. Shinaoka, Y. Tomita, and Y. Motome, Phys. Rev. Lett. **107**, 047204 (2011).
[110] C. Escorihuela-Sayalero, O. Diéguez, and J. Íñiguez, Phys. Rev. Lett. **109**, 247202 (2012).
[111] D. Boldrin *et al.*, Adv. Funct. Mater. **29**, 1902502 (2019).
[112] S.-Y. Zhang, Y.-H. Lin, C.-W. Nan, R. Zhao, and J. He, J. Am. Ceram. Soc. **91**, 3263 (2008).
[113] T. Ogawa, H. Nagasaki, and T. Sato, Phys. Rev. B **65**, 024430 (2001).
[114] A. A. Bokov and Y. G. Ze, *Nanoscale Ferroelectrics and Multiferroics: Key Processing and Characterization Issues, and Nanoscale Effects* (John Wiley & Sons, Hoboken, NJ, 2016), Vol. 2, Chap. 23.
[115] J. R. Thomson, H. Guo, D. H. Ryan, M. J. Zuckermann, and M. Grant, Phys. Rev. B **45**, 3129 (1992).

[116] K. Binder and A. P. Young, Rev. Mod. Phys. **58**, 801 (1986).
[117] J. Alonso, M. L. Fdez-Gubieda, J. M. Barandiarán, A. Svalov, L. F. Barquín, D. A. Venero, and I. Orue, Phys. Rev. B **82**, 054406 (2010).
[118] G. Burns and F. H. Dacol, Solid State Commun. **48**, 853 (1983).
[119] B. Jaffe, W. R. Cook, and H. Jaffe, *Piezoelectric Ceramics* (Elsevier, New York, 1971).
[120] S. A. Mabud and A. M. Glazer, J. Appl. Crystallogr. **12**, 49 (1979).
[121] P. J. Phillips, M. De Graef, L. Kovarik, A. Agrawal, W. Windl, and M. Mills, Ultramicroscopy **116**, 47 (2012).
[122] C.-H. Lee *et al.*, Nature (London) **502**, 532 (2013).
[123] L. Zhang *et al.*, Science **361**, 494 (2018).
[124] J.-S. Lee, Y. W. Xie, H. K. Sato, C. Bell, Y. Hikita, H. Y. Hwang, and C.-C. Kao, Nat. Mater. **12**, 703 (2013).
[125] T. Shimada, Y. Uratani, and T. Kitamura, Appl. Phys. Lett. **100**, 162901 (2012).
[126] T. Shimada, J. Wang, Y. Araki, M. Mrovec, C. Elsässer, and T. Kitamura, Phys. Rev. Lett. **115**, 107202 (2015).
[127] L. Zhang *et al.*, Nano Lett. **20**, 881 (2019).